

THE BLAZAR SEQUENCE AND THE COSMIC GAMMA-RAY BACKGROUND RADIATION IN THE FERMI ERA

YOSHIYUKI INOUE AND TOMONORI TOTANI

Department of Astronomy, Kyoto University, Kitashirakawa, Sakyo-ku, Kyoto 606-8502, Japan

Draft version January 26, 2023

ABSTRACT

We present a new model of the blazar gamma-ray luminosity function (GLF) and the spectrum of the extragalactic gamma-ray background (EGRB), which is consistent with the observed distributions of EGRET blazars. The unified sequence of blazar spectral energy distribution (SED) is taken into account to make a non-trivial prediction for the EGRB spectrum and more realistic comparison with the data than previous studies. We then try to explain the EGRB data by the two AGN populations: one is blazars, and the other is non-blazar AGNs that are responsible for the EGRB in the MeV band. We find that $\sim 80\%$ of the EGRB photon flux at > 100 MeV can be explained by this model, which is a significantly higher fraction than previous studies. The predicted EGRB spectrum is in agreement with a wide range of the observed data from X-ray to GeV, within the systematic uncertainties in the EGRB determination by EGRET. These results indicate that AGNs including blazars are the primary source of EGRB. Blazars are dominant in EGRB at higher energy bands of $\gtrsim 100$ MeV, while non-blazar AGNs dominate at $\lesssim 100$ MeV. Almost all of the EGRB flux from blazars will be resolved into discrete sources by the *Fermi* Gamma-ray Space Telescope, while that from non-blazar AGNs will largely remain unresolved. Therefore, comparison between the integrated source counts and diffuse EGRB flux as a function of photon energy will give a simple and clear test of our model. Various quantitative predictions for *Fermi* observations are also made. Especially, our model predicts 600–1200 blazars in all sky down to 2×10^{-9} photons $\text{cm}^{-2}\text{s}^{-1}$ (> 100 MeV), which is considerably smaller than previous studies. We find that the fraction of EGRB energy flux absorbed in intergalactic medium (IGM) is not large, and the cascade component reprocessed in IGM does not significantly alter the EGRB spectrum.

Subject headings: cosmology: diffuse radiation – galaxies : active – gamma rays : theory

1. INTRODUCTION

The origin of the extragalactic diffuse gamma-ray background (EGRB) has been discussed in astrophysics for a long time. EGRB was first discovered by the SAS 2 satellite (Fichtel, Simpson, & Thompson 1978; Thompson & Fichtel 1982). Subsequently, the EGRB spectrum was confirmed up to ~ 50 GeV by EGRET (Energetic Gamma-Ray Experiment Telescope) on board the Compton Gamma Ray Observatory. The EGRB flux is about 1×10^{-5} photons $\text{cm}^{-2} \text{s}^{-1} \text{sr}^{-1}$ above 100 MeV and the spectrum is approximately a power law with a photon index of ~ -2 in a wide range of ~ 30 MeV – 100 GeV (Sreekumar et al. 1998; Strong, Moskalenko, & Reimer 2004a). It should be noted that, however, measurement of EGRB is not an easy task. The Galactic diffuse background from cosmic-ray interaction in the Galactic disk is a strong *foreground* emission and must be subtracted to estimate EGRB. Therefore modeling of this foreground component could induce significant systematic uncertainties in EGRB measurements (Keshet, Waxman, & Loeb 2004; Strong, Moskalenko, & Reimer 2004a,b; Kamae, Abe, & Koi 2005; Kamae et al. 2006). A possible systematic error in the calibration of the EGRET detector may also have affected the EGRB determination (Stecker et al. 2008).

Although several sources of gamma-rays (e.g., clusters of galaxies or dark matter annihilation) have been proposed as a significant contributor to EGRB [see, e.g., Narumoto & Totani (2006) and references therein], active galactic nuclei (AGNs) of the blazar class have been thought as the primary candidate for the origin of EGRB, since almost all of the extragalactic gamma-ray sources detected by EGRET are blazars. The

blazar contribution to EGRB has been estimated by a number of papers (Padovani et al. 1993; Stecker, Salamon, & Malkan 1993; Salamon & Stecker 1994; Chiang et al. 1995; Stecker & Salamon 1996; Chiang & Mukherjee 1998; Mücke & Pohl 2000; Narumoto & Totani 2006; Giommi et al. 2006; Dermer 2007; Pavlidou & Venters 2008; Kneiske & Mannheim 2008) by various methods and modelings.

Stecker & Salamon (1996) estimated that 100% of the EGRB radiation can be explained by blazars. However, their model was constructed based on the blazar luminosity function (LF) in radio bands, without statistical comparison with the gamma-ray flux and redshift distributions of the EGRET blazars. Therefore it was not certain whether their model was statistically consistent with the EGRET blazar data. Chiang & Mukherjee (1998) constructed a model of blazar gamma-ray luminosity function (GLF) that is consistent with the EGRET blazar data (flux and redshift), and found that only 25% of EGRB can be accounted for by blazars. A similar conclusion was obtained by an independent study by Mücke & Pohl (2000). These studies considered only the pure luminosity evolution (PLE) of blazar GLF, based on the radio luminosity function of blazars.

Narumoto & Totani (2006, hereafter NT06) extended this kind of analysis by introducing a new evolutionary history of AGNs revealed by more recent X-ray observations. They constructed a new GLF model based on a luminosity-dependent density evolution (LDDE), which has been known to describe well the evolution of X-ray luminosity function (XLF) of AGNs. NT06 found that the LDDE model fits to the EGRET blazar data better than PLE models. It is then confirmed again that only 25–50% of EGRB can be explained by blazars, with a better knowledge of AGN evolution. In most of these

studies, however, blazar spectral energy distributions (SEDs) were assumed to be a single or broken power-law for all blazars. In such a modeling, the predicted EGRB spectrum is almost obviously determined by the assumed power-law indices. Mücke & Pohl (2000) used the theoretical blazar emission model of Dermer & Schlickeiser (1993), in which the blazar SED changes with luminosity. However, the SED model was constructed without taking into account the observed trend of the blazar SED described below, and the expected EGRB spectrum by their model was not presented or discussed in the paper.

Blazar SED has been theoretically and observationally studied in detail (Ghisellini & Tavecchio 2008, and references therein). From the theoretical point of view, blazar emission is widely believed to be the sum of the synchrotron (radio to UV bands) and inverse Compton (dominant in gamma-ray bands) components produced by the same nonthermal electron population accelerated in relativistic jets. The source of target photons for the inverse-Compton (IC) component could be either the synchrotron photons produced in the jet itself (synchrotron-self-Compton, SSC), or photons emitted from the accretion disk. Multi-wavelength observational studies from radio to γ -ray bands have indicated an interesting feature in blazar SEDs; the synchrotron and Compton peak photon energies decrease as the bolometric luminosity increases (Fossati et al. 1997, 1998; Donato et al. 2001, Ghisellini & Tavecchio 2008, Maraschi et al. 2008; but see also Padovani et al. 2007). This is often called as the blazar SED sequence. Although the validity of the blazar sequence is currently still a matter of debate (e.g., Padovani et al. 2007; Ghisellini & Tavecchio 2008; Maraschi et al. 2008), one can make a non-trivial prediction of the EGRB spectrum if this blazar sequence is assumed. In other words, the blazar SED sequence can be tested by comparing with the observed EGRB spectrum.

In this paper we calculate the EGRB flux and spectrum from blazars, by constructing a blazar GLF model that is consistent with the flux and redshift distributions of the EGRET blazars, based on the LDDE scheme and the blazar SED sequence. By introducing the blazar SED sequence, we can make a reasonable and non-trivial prediction of the EGRB spectrum for the first time, which can be compared with the observed EGRB spectrum. Recently, Inoue, Totani, & Ueda (2008) has showed that EGRB in the MeV band can naturally be explained by normal (i.e., non-blazar) AGNs that compose the cosmic X-ray background. This MeV background component extends to ~ 100 MeV with a photon index of about 2.8, by the Comptonization photons produced by non-thermal electrons in hot coronae. Therefore, it should also contribute to the EGRB at $\lesssim 1$ GeV. We will investigate how much fraction of the observed EGRB can be explained by the sum of the two components, i.e., non-blazar AGNs (dominant at $\lesssim 100$ MeV) and blazars (dominant at $\gtrsim 100$ MeV). We will also make quantitative predictions for the *Fermi* Gamma-ray Space Telescope (formerly known as GLAST) that has successfully been launched on June 11th, 2008.

This paper is organized as follows. In §2, we present the treatment of the blazar SED sequence in our calculation. We describe the formulations for the blazar GLF model taking into account the SED sequence in §3, and the parameter determination by fitting to the EGRET data in §4. The EGRB is calculated and compared with the observed data in §5, and we present predictions for *Fermi* in §6. Conclusions are given in §7. Throughout this paper, we adopt the standard cosmologi-

cal parameters of $(h, \Omega_M, \Omega_\Lambda) = (0.7, 0.3, 0.7)$.

2. THE BLAZAR SED SEQUENCE

Fossati et al. (1997, 1998) and Donato et al. (2001, hereafter D01) constructed an empirical blazar SED model to describe the SED sequence, based on fittings to observed SEDs from radio to γ -ray bands. These models are comprised of the two components (synchrotron and IC), and each of the two is described by a linear curve at low photon energies and a parabolic curve at high energies, in the plane of $\log_{10}(\nu L_\nu)$ and $\log_{10} \nu$.

Here we construct our own SED sequence model mainly based on the SED model of D01, because there is a mathematical discontinuity in the original D01 model. In the D01 model, two different mathematical fitting formulae are used below and above the luminosity $\nu L_\nu = 10^{43}$ erg s $^{-1}$ at 5 GHz, and the luminosity of the inverse-Compton component suddenly changes with a jump at this critical luminosity. Our own SED sequence formula is described in Appendix in detail, and the discontinuity is avoided there. Once the blazar luminosity is specified at a reference frequency (e.g., 5 GHz in radio band), this empirical model gives the full blazar SED from radio to gamma-ray bands. In Fig.1 we show this empirical blazar SED sequence model in comparison with the observed SED data (Fossati et al. 1998; D01). It should be noted that the observed data are means of many blazars in a certain luminosity range. When the bolometric blazar luminosity $P \equiv \int \nu L_\nu$ is specified, the blazar luminosity per unit frequency, $L_\nu(\nu, P)$, is determined for any photon frequency ν by the blazar sequence model.

3. THE MODEL OF GAMMA-RAY LUMINOSITY FUNCTION OF BLAZARS

3.1. Relating Jet Power and X-ray Luminosity of AGNs

The cosmological evolution of X-ray luminosity function of AGNs has been investigated intensively [Ueda et al. 2003 (hereafter U03); Hasinger, Miyaji, & Schmidt 2005 (hereafter H05); Sazonov et al. 2007; Gilli, Comastri, & Hasinger 2007]. These studies revealed that AGN XLF is well described with the LDDE model, in which peak redshift of density evolution increases with AGN luminosity. Here we construct two models of blazar GLF based on the two XLFs derived by U03 (in hard X-ray band) and H05 (in soft X-ray band), both of which are based on the LDDE scheme. It is natural to expect that power of blazar jet is correlated with mass accretion rate to super massive black holes, which is also correlated with the X-ray luminosity from accretion disk. Therefore we simply assume that the bolometric luminosity of radiation from jet, P , is proportional to disk X-ray luminosity, L_X . It should be noted that L_X is *not* the observed X-ray luminosity of a blazar having a jet luminosity P ; when an AGN is observed as a blazar (i.e., the jet directed to an observer), its X-ray flux is dominated by the radiation from the jet that is much brighter than that from the accretion disk. The use of LDDE in blazar GLF has been supported from the EGRET blazar data, because NT06 found that the EGRET data agrees with the LDDE model better than PLE models. However, the validity of this assumption from a theoretical viewpoint should be more carefully examined.

A constant P/L_X ratio is realized when, e.g., a universal fraction of AGNs show jet activity, and the jet kinetic luminosity is proportional to X-ray luminosity. One should, however, be careful about the latter condition. Recent observations of X-ray binaries indicate that the jet kinetic luminosity

is generally proportional to the accretion rate (\dot{m}), but X-ray luminosity is not, when the accretion rate is much lower than the Eddington limit (i.e., low Eddington ratio) (Gallo et al. 2003; Gallo et al. 2005). Such accretion disks are described by radiatively inefficient accretion flows (RIAF) rather than the standard accretion disk, and X-ray luminosity is roughly proportional to \dot{m}^2 in the RIAF regime (Kato et al. 1998; Narayan & Quataert 2005). The RIAF picture is well consistent with the accretion flow onto the supermassive black hole of the Galaxy (i.e., Sgr A*) (see, e.g., Totani 2006 and references therein).

Accretion rates of X-ray bright AGNs used to derive the AGN XLF are generally close to the Eddington limit, otherwise they are hardly detected by X-ray observations because of the rapid decrease of X-ray luminosity with decreasing Eddington ratio. Therefore, our blazar GLF should be considered as that for high Eddington ratio AGNs, and low Eddington-ratio AGNs in the RIAF regime could be missed in our analysis. Such a population might have a significant contribution to blazar GLF, because the jet activity is expected to be proportional to accretion rate, in contrast to disk X-ray luminosity $L_X \propto \dot{m}^2$ in the RIAF mode. However, the black hole mass function predicted by time integration of X-ray AGN LF is consistent with the local black hole mass function inferred from the black-hole-mass versus bulge-mass relation, indicating that black hole mass grows mainly in the high Eddington ratio phase (Marconi et al. 2004). If this is correct, background radiation from accretion onto AGN black holes should be dominated by those in high Eddington ratio phase. Hence, it is reasonable to expect that a significant part of EGRB flux can be accounted for by blazars with high Eddington ratio phase, whose GLF evolution is described by LDDE.

3.2. Model Formulations

In this paper we describe the blazar GLF in terms of νL_ν luminosity at a reference rest-frame photon energy $\epsilon_{\text{ref, res}} \equiv 100$ MeV, i.e., $L_\gamma \equiv (\epsilon_{\text{ref, res}}/h_p) L_\nu(\epsilon_{\text{ref, res}}/h_p, P)$, where h_p is the Planck constant. According to the assumption justified in §3.1, we simply relate the bolometric blazar luminosity P and disk X-ray luminosity by the parameter q , as:

$$P = 10^q L_X. \quad (1)$$

Here, we define the disk luminosity L_X to be that in the rest-frame 2–10 and 0.5–2 keV bands for the hard XLF (U03) and the soft XLF (H05), respectively. Thus, L_γ and L_X have been related through P .

The blazar GLF is then obtained from the AGN XLF, as

$$\rho_\gamma(L_\gamma, z) = \kappa \frac{dL_X}{dL_\gamma} \rho_X(L_X, z), \quad (2)$$

where ρ_X and ρ_γ are the XLF and GLF, i.e., the comoving number densities of X-ray AGNs and blazars per unit X-ray and gamma-ray luminosity, respectively. The parameter κ is a normalization factor, representing the fraction of AGNs observed as blazars. In our GLF model, we adopt the same form in U03 and H05 for ρ_X , as:

$$\rho_X(L_X, z) = \rho_X(L_X, 0) f(L_X, z), \quad (3)$$

where $\rho_X(L_X, 0)$ is the AGN XLF at present. This is characterized by the faint-end slope index γ_1 , the bright-end slope index γ_2 , and the break luminosity L_X^* , as:

$$\rho_X(L_X, 0) = \frac{A_X}{L_X \ln(10)} \left[\left(\frac{L_X}{L_X^*} \right)^{\gamma_1} + \left(\frac{L_X}{L_X^*} \right)^{\gamma_2} \right]^{-1}, \quad (4)$$

TABLE 1
THE PARAMETERS OF THE AGN XLF

	Ueda et al. 2003	Hasinger et al. 2005
A_X^a	5.04×10^{-6}	2.62×10^{-7}
$\log_{10} L_X^{*b}$	$43.94^{+0.21}_{-0.26}$	43.94 ± 0.11
γ_1	0.86 ± 0.15	0.87 ± 0.10
γ_2	2.23 ± 0.13	2.57 ± 0.16
z_c^*	1.9^c	1.96 ± 0.15
$\log_{10} L_a^b$	44.6^c	44.67^c
α	0.335 ± 0.07	0.21 ± 0.04
p_1^*	4.23 ± 0.39	4.7 ± 0.3
p_2^*	-1.5^c	-1.5 ± 0.7
β_1	0.0^d	0.7 ± 0.3
β_2	0.0^d	0.6 ± 0.8

^a In units of Mpc^{-3} .

^b In units of ergs s^{-1} .

^c These quantities are treated as fixed parameters in each XLF model.

^d The indices β_1, β_2 are treated as constants in U03.

where A_X is the normalization parameter having a dimension of volume^{-1} . The function $f(L_X, z)$ describes the density evolution, which is given by the following forms:

$$f(L_X, z) = \begin{cases} (1+z)^{p_1} & z \leq z_c(L_X), \\ f(L_X, z_c(L_X)) \left(\frac{1+z}{1+z_c(L_X)} \right)^{p_2} & z > z_c(L_X), \end{cases} \quad (5)$$

where z_c is the redshift of evolutionary peak, given as

$$z_c(L_X) = \begin{cases} z_c^* & L_X \geq L_a, \\ z_c^*(L_X/L_a)^\alpha & L_X < L_a, \end{cases} \quad (6)$$

The evolutionary indices p_1 and p_2 are described by using the parameters p_1^*, p_2^*, β_1 , and β_2 :

$$p_1 = p_1^* + \beta_1(\log_{10} L_X - 44.0), \quad (7)$$

$$p_2 = p_2^* + \beta_2(\log_{10} L_X - 44.0). \quad (8)$$

The parameters obtained by the fit to the observed data of X-ray AGNs in U03 and H05 are shown in Table 1.

When we calculate the EGRB flux, it diverges if $\gamma_1 > 1$ and GLF is integrated down to $L_\gamma \rightarrow 0$. Therefore we set the minimum of the gamma-ray luminosity as $L_{\gamma, \text{min}} = 10^{43} \text{ erg s}^{-1}$ in the EGRB calculation, because we will find that there is no EGRET blazars below this value (see Fig. 2). However, it should be kept in mind that there might be a considerable contribution to the EGRB flux from blazars below $L_{\gamma, \text{min}}$ when $\gamma_1 > 1$.

4. GAMMA-RAY LUMINOSITY FUNCTION DETERMINED BY THE EGRET BLAZAR DATA

4.1. The Maximum Likelihood Method

We use the maximum likelihood method to search for the best-fit model parameters of the blazar GLF to the distributions of the observed quantities of the EGRET blazars (gamma-ray flux and redshift). The analysis method and the data used are essentially the same as those in NT06.

Observed gamma-ray flux F_γ of EGRET blazars are photon flux at $\epsilon_\gamma \geq \epsilon_{\text{min, obs}} \equiv 100$ MeV in photons $\text{cm}^{-2} \text{ s}^{-1}$, where $\epsilon_{\text{min, obs}}$ is in the observer's frame. For a given redshift, F_γ can be related to P by the blazar SED sequence model as follows:

$$F_\gamma = \frac{1+z}{4\pi d_L(z)^2} \int_{\epsilon_{\text{min, obs}}(1+z)/h_p}^{\infty} \frac{L_\nu(\nu, P)}{h_p \nu} d\nu, \quad (9)$$

where z is redshift and $d_L(z)$ the standard luminosity distance. Since P has been related to the gamma-ray luminosity L_γ by the SED sequence, one can calculate $L_\gamma(z, F_\gamma)$ for a given set of z and F_γ through P .

A specified GLF model predicts the distribution function $d^3N/dz dF_\gamma d\Omega$ of redshift z , flux F_γ , and the location of a blazar in the sky specified by a solid angle Ω , which is given as:

$$\frac{d^3N(z_i, F_{\gamma,i}, \Omega_i)}{dz dF_\gamma d\Omega} = \frac{dV}{dz} \rho_\gamma(L_\gamma, z) \epsilon(F_\gamma, z) \times \Theta[F_\gamma - F_{\gamma,\text{lim}}(\Omega)], \quad (10)$$

where dV/dz is the comoving volume element per unit solid angle, Θ the step function ($\Theta(x) = 1$ and 0 for $x \geq 0$ and $x < 0$, respectively), and $F_{\gamma,\text{lim}}(\Omega)$ the sensitivity limit of EGRET for point sources that is a function of the Galactic latitude. The functional form of $F_{\gamma,\text{lim}}(\Omega)$ is given in NT06. The detection efficiency $\epsilon(F_\gamma, z)$ represents the identification probability as a blazar by finding a radio counterpart. This is described §2.3 in NT06, but here we modified the relation between L_R and L_γ from a simple linear relation in NT06 to that predicted from our blazar SED sequence model. As in NT06, we also take into account a log-normal scatter around the mean relation of L_R/L_γ with a standard deviation of $\sigma_p = 0.49$ in $\log_{10}(L_R/L_\gamma)$. It should be noted that the blazar SED sequence is an averaged SED for groups of blazars binned according to radio luminosity, and some scatter of L_R/L_γ is expected for individual blazars.

The likelihood function is given by

$$\mathcal{L} = \prod_{i=1}^{N_{\text{obs}}} \left[\frac{1}{N_{\text{exp}}} \frac{dN(z_i, F_{\gamma,i}, \Omega_i)}{dz dF_\gamma d\Omega} \right], \quad (11)$$

where the subscript i is identification of each blazar, N_{obs} the observed number of blazars, and N_{exp} the expected number of the blazar detections, i.e.,

$$N_{\text{exp}} = \int dz \int dF_\gamma \int d\Omega \frac{d^3N}{dz dF_\gamma d\Omega}. \quad (12)$$

The likelihood function does not depend on the normalization of GLF, and the normalization parameter κ is determined by requiring $N_{\text{exp}} = N_{\text{obs}}$. There are $N_{\text{obs}} = 46$ blazars in the sample analyzed in NT06 and this work.

4.2. The Best Fit Parameters

In the first analyses, we take q as the only one free parameter of the blazar GLF, with all the XLF model parameters fixed at the values of U03 and H05. These are hereafter called as U03(q) and H05(q) fits, respectively. In the second analyses, we take the faint-end slope index of XLF γ_1 as another free parameter in addition to q . These are hereafter called as U03(q, γ_1) and H05(q, γ_1) fits, respectively. The best-fit values for these four fits are shown in Table. 2. Figure 2 shows the distributions of redshift and gamma-ray luminosity predicted by the best-fit models, in comparison with the EGRET data. We obtained the best-fit values of $q \sim 5$, meaning that the observed jet luminosity P (bolometric blazar luminosity) is typically 10^5 higher than the disk X-ray luminosity. In the U03(q, γ_1) model, the characteristic AGN X-ray luminosity L_X^* (the break in XLF) corresponds to the blazar gamma-ray luminosity of $L_\gamma^* = 10^{48}$ erg s $^{-1}$.

We performed the Kolmogorov-Smirnov (KS) test to see the goodness of fits for the best-fit results of each of the

TABLE 2
BEST-FIT PARAMETERS FOR BLAZAR GLF

	U03(q)	U03(q, γ_1)	H05(q)	H05(q, γ_1)
q	$4.92^{+0.21}_{-0.10}$	$4.93^{+0.25}_{-0.10}$	$5.29^{+0.26}_{-0.22}$	$5.35^{+0.25}_{-0.21}$
γ_1	0.86^a	0.93 ± 0.13	0.87^a	$1.11^{+0.11}_{-0.12}$
κ	1.7×10^{-6}	1.5×10^{-6}	9.5×10^{-6}	6.0×10^{-6}
KS test probabilities				
z	53.8%	86.9%	0.15%	33.0%
L_γ	25.6%	48.4%	0.08%	28.5%

NOTE. — The best-fit values of the model parameters (q, γ_1, κ) obtained from the maximum likelihood analysis. The KS probabilities of the best-fit models are also shown for the redshift and gamma-ray luminosity distributions in the last two rows.

^a These parameters are fixed at the original AGN XLF values in these analysis, and the fixed values are shown.

four fits, and the chance probabilities of getting the observed KS deviation are shown in Table 2. Except for the H05(q) model, the fits are statistically acceptable. Since the best KS test value is obtained for the U03(q, γ_1) GLF model, we use the U03(q, γ_1) GLF model as the baseline below, when only one of the four fits is presented. In Fig. 3 we show the allowed regions of the model parameters in the U03(q, γ_1) and H05(q, γ_1) models. The best-fit value of γ_1 in the U03(q, γ_1) model is in good agreement with the original value derived by U03. The value in the H05(q, γ_1) model is slightly larger than the original H05 value, but the statistical significance is not large. The difference between the U03(q, γ_1) and H05(q, γ_1) fits may be a result of different selections of AGNs in soft (H05) and hard X-ray (U03) bands, because strongly obscured AGNs would more easily be missed in soft X-ray bands than in hard X-ray bands.

It should be noted that the results of the acceptable KS probabilities and the similar γ_1 values to the original XLFs give some support to our basic assumption of a simple proportionality between the X-ray accretion luminosity and the jet luminosity. As mentioned above, AGNs with faint accretion X-ray luminosity may be in the RIAF mode (low-Eddington ratio) rather than the standard disk mode, where X-ray luminosity from accretion flow is not simply proportional to the mass accretion rate or the jet luminosity. This implies that the EGRET data can be described well with the assumption that the majority of EGRET blazars are in the standard disk mode or high Eddington ratio phase.

5. THE GAMMA-RAY BACKGROUND SPECTRUM

5.1. the EGRB Spectrum Calculation

We calculate the EGRB spectrum by integrating our blazar SED sequence model in the redshift and luminosity space, using the blazar GLF derived in §3. The spectrum of EGRB radiation (photon flux per unit photon energy and per steradian) is calculated as

$$\begin{aligned} \frac{d^2F(\epsilon_\gamma)}{d\epsilon_\gamma d\Omega} &= \frac{c}{4\pi} \int_0^{z_{\text{max}}} dz \frac{dt}{dz} \int_{L_{\text{min}}}^{L_{\text{max}}} dL_\gamma \rho_\gamma(L_\gamma, z) \\ &\times \frac{(1+z)}{h_p} \frac{L_\nu[\epsilon_\gamma(1+z)/h_p, P(L_\gamma)]}{\epsilon_\gamma(1+z)} \\ &\times e^{-\tau_{\gamma\gamma}(z, \epsilon_\gamma)}, \end{aligned} \quad (13)$$

where ϵ_γ is the observed gamma-ray photon energy, t the cosmic time, and dt/dz can be calculated by the Friedmann

equation in the standard cosmology. We assume $z_{\text{max}} = 5$ in this calculation, but the EGRB flux is hardly dependent on this parameter, since the peak of GLF/XLF evolution is well below $z \sim 5$. The gamma-ray luminosity minimum is set at $L_{\gamma, \text{min}} = 10^{43} \text{ erg s}^{-1}$ as mentioned earlier, and we set $L_{\gamma, \text{max}} = 10^{50} \text{ erg s}^{-1}$ because blazars brighter than this luminosity are not known, although the EGRB flux hardly depends on $L_{\gamma, \text{max}}$.

Very high energy photons ($> 20 \text{ GeV}$) from high redshift are absorbed by the interaction with the cosmic infrared background (CIB) radiation (Salamon & Stecker 1998; Totani & Takeuchi 2002; Kneiske et al. 2004; Stecker, Malkan, & Scully 2006), and $\tau_{\gamma\gamma}(z, \epsilon_{\gamma})$ is the optical depth of the universe against this reaction. In this paper, we adopt the model of Totani & Takeuchi (2002) for CIB and $\tau_{\gamma\gamma}$. The gamma-ray absorption produces electron-positron pairs, and the pairs would scatter the cosmic microwave background (CMB) radiation to make the secondary contribution (the cascade component) to high energy background radiation (Aharonian et al. 1994; Fan et al. 2004). We take into account this cascading emission to calculate EGRB spectrum, considering only the first generation of created pairs, by using the same formulations in Kneiske & Mannheim (2008). In the following results, we will find that the amount of energy flux absorbed and reprocessed in intergalactic medium (IGM) is only a small fraction of the total EGRB energy flux, and hence the model dependence of CIB or the treatment of the cascading component does not have serious effects on our conclusions in this work.

5.2. The EGRB Spectrum from Blazars

Figure 4 shows the νF_{ν} EGRB spectrum predicted by the best-fit GLF model parameters obtained above. Here, we show the total EGRB flux as well as the contributions from different L_{γ} ranges. This EGRB spectrum is the primary spectrum directly from blazars, because in this calculation the effect of photon absorption in IGM is included but the cascade emission is not. The data of SMM (Watanabe et al. 1999), COMPTEL (Kappadath et al. 1996) and EGRET (Sreekumar et al. 1998; Strong et al. 2004a) are also shown. As seen in Figure 4, the contribution from low-luminosity blazars with $\log_{10}(L_{\gamma}/\text{erg s}^{-1}) = 43\text{--}45$ is significant only above 1 GeV, because of the assumed SED sequence of blazars. The contribution from these low-luminosity blazars is larger in the model of H05(q, γ_1) than that of H05(q), because the faint-end slope of the GLF becomes steeper when γ_1 is treated as a free parameter.

An important implication here is that the contribution from the so-called MeV blazars, which have their SED peaks at around MeV, is negligible in the MeV gamma-ray background flux, although such MeV blazars have been suspected as a possible origin of the MeV background. This is because MeV blazars have a large luminosity of $\log_{10}(L_{\gamma}/\text{erg s}^{-1}) = 49\text{--}50$ in the blazar SED sequence, and the number density of such blazars is small.

Figure 5 shows the intrinsic (the spectrum without taking into account the absorption by CIB), absorbed (the same as Fig. 4), and cascading components of EGRB spectrum, as well as the total (absorbed+cascade) spectrum. The absorption by CIB becomes significant at $\epsilon_{\gamma} \gtrsim 100 \text{ GeV}$, and the absorbed EGRB photons are converted into lower energy gamma-rays, with the energy flux roughly conserved. However, the absorbed energy flux of EGRB above $\sim 100 \text{ GeV}$ is not significantly larger than the unabsorbed energy flux, and

hence the increase of EGRB flux or change of the EGRB spectrum at $\lesssim 100 \text{ GeV}$ by the cascading component is not a large effect.

5.3. The EGRB Spectrum from Non-blazar AGNs

In addition to blazars, we take into account non-blazar AGNs as the source of EGRB. Inoue et al. (2008, hereafter ITU08) has shown that non-blazar AGNs are a promising source of EGRB at $\sim 1\text{--}10 \text{ MeV}$. In this scenario, a nonthermal power-law component extends from hard X-ray to $\sim 10 \text{ MeV}$ band in AGN spectra, because of nonthermal electrons that is assumed to exist ubiquitously in hot coronae around AGN accretion disks. The existence of such nonthermal electrons is theoretically reasonable, because the hot coronae are the essential component in the standard picture of X-ray emission from AGNs, and magnetic reconnection is the promising candidate for the heating source of the hot coronae (Laor & Behar 2008). Magnetic reconnections should produce non-thermal particles as known in e.g., solar flares or the earth magnetosphere. Although several sources have been proposed as the origin of the MeV background, this model gives the most natural explanation for the observed MeV background spectrum that is a simple power-law smoothly connected to CXB.

Theoretically, there is no particular reason to expect a cut-off of the nonthermal emission around 10 MeV, and it is well possible that this emission extends beyond 10 MeV with the same power index. Then, this component could make some contribution to EGRB in the EGRET energy band. The EGRB spectrum from the non-blazar AGNs calculated based on the model of ITU08 is shown in Figure 6, in comparison with the blazar component. There is some discrepancy between the MeV EGRB data of SMM and COMPTEL, and the reason for this is not clear. Here we use two model parameter sets of $(\Gamma, \gamma_{\text{tr}}) = (3.5, 4.4)$ and $(3.8, 4.4)$ in ITU08, where Γ is the power-law index of nonthermal electron energy distribution and γ_{tr} is the transition electron Lorentz factor above which the nonthermal component becomes dominant. These two parameter sets are chosen so that they fit to the COMPTEL and SMM data, respectively. The EGRB flux is dominated by blazars at the energy range above $\sim 100 \text{ MeV}$, while the non-blazar component is dominant at the lower photon energies.

5.4. On the Origin of EGRB

As can be seen in Fig. 6, the overall background spectrum from X-ray to 1 GeV predicted by our blazar plus non-blazar model is similar to the observed data. Especially, the EGRB prediction using the H05(q, γ_1) blazar GLF model and the ITU08 non-blazar background model with $\Gamma = 3.5$ is in nice agreement with the observed data of Strong et al. (2004a) in 0.1–1 GeV. In this case, the predicted EGRB flux at 100 MeV can account for 80% of the observed flux, which is a considerably higher fraction than those in previous studies (Chiang & Mukherjee 1998; Mücke & Pohl 2000; NT06). It should be noted that the contribution to the EGRB flux at 100 MeV from blazars is $\sim 30 \%$, which is similar to those estimated by previous studies. The high fraction is due to the EGRB component from non-blazar AGNs.

The prediction is still 20 % short of the observed flux, and the discrepancy becomes more serious when the model is compared with the Strong et al. (2004a) data above 1 GeV or with the original EGRB determination by the EGRET team (Sreekumar et al. 1998). Especially, the apparent excess of

the observed EGRB flux beyond 1 GeV might be a contribution from a completely different component, e.g., dark matter annihilation (e.g., Oda, Totani, & Nagashima 2005). Therefore we carefully discuss the possible origin of the discrepancy below.

We should first examine the uncertainties in the model prediction. Since the GLF likelihood determination is based only on 46 blazars, there is a statistical uncertainty of 15 and 32% in the normalization of GLF and the EGRB flux at 68 and 95% C.L., respectively. The sensitivity limit of EGRET has been included in the GLF likelihood analysis. The EGRET sensitivity to a point source changes depending on the location in the sky, and we used sensitivity limit inferred from the signal-to-noise ratios of the EGRET sources as a function of the Galactic latitude, as in NT06. The sensitivity limit has a $\sim 30\%$ scatter even after binned by the Galactic latitude. When the sensitivity limit is changed by $\pm 30\%$, we find that the GLF normalization and EGRB flux changes by $\pm \sim 25\%$. Since the faint-end slopes of the (q, γ_1) GLF models are $\gamma_1 \sim 1$, the faint-end cut-off luminosity $L_{\gamma, \min}$ of blazar GLF could also be important. We therefore repeated the calculation with $L_{\gamma, \min}$ changed by a factor of 10 from the baseline model, but we find that the EGRB flux changes by only $\sim 0.8\%$ and $\sim 1.7\%$ for $U03(q, \gamma_1)$ and $H05(q, \gamma_1)$, respectively. Therefore, our result is not sensitive to $L_{\gamma, \min}$.

Next we examine the possible systematic uncertainties in the observational determination of EGRB. The correct modeling of the foreground, i.e., the Galactic diffuse emission is critical for the EGRB measurement. However, there is a well-known problem of “GeV anomaly”, which is an excess of the observed diffuse flux compared with the standard theoretical model of the Galactic diffuse emission (Pohl & Esposito 1998; Strong et al. 2004b; de Boer et al. 2005; Kamae, Abe, & Koi 2005; Stecker, Hunter, & Kniffen 2008). The difference of the EGRB data of Strong et al. (2004a) from the original EGRET data (Sreekumar et al. 1998) is a result of modifying the model of the Galactic diffuse emission to resolve the GeV anomaly, demonstrating that theoretical uncertainties in the Galactic diffuse emission could have a significant effect on the EGRB measurements. On the other hand, Stecker et al. (2008) suggested that the most likely cause of the GeV anomaly is a systematic error in the calibration of the EGRET detector at photon energies beyond 1 GeV, and they derived the correction factors for the flux measured by EGRET. If their claim is correct, the correction factors should be multiplied to the original EGRET measurements of EGRB (Sreekumar et al. 1998), and such corrected data are shown and compared with the models in Fig. 7. Although the overall corrected EGRB flux is still higher than the model predictions, the corrected spectrum is similar to those of models. The marked dip at ~ 1 GeV and hump at higher photon energies found in the data of Strong et al. (2004a) are not seen. It should also be noted that the EGRET EGRB data at ~ 50 GeV is considerably higher than the neighboring COMPTEL data, again indicating some systematic uncertainties in the EGRB flux estimates.

Based on these results and considerations, we conclude that most, and probably all, of the EGRB flux can be explained by blazars and non-blazar AGNs, with luminosity functions that are consistent with the EGRET blazar data and the X-ray AGN surveys. However, we should await the *Fermi* measurement of EGRB to examine whether we need still different sources of EGRB with higher accuracy.

6. PREDICTIONS FOR THE *FERMI* MISSION

6.1. Expected Number of Blazars and Non-blazar AGNs

The left panel of Figure 8 shows the cumulative distribution of > 100 MeV photon flux of blazars. The four GLF models of $U03(q)$, $U03(q, \gamma_1)$, $H05(q)$, and $H05(q, \gamma_1)$, predict that about 640, 930, 470, and 1200 blazars should be detected by *Fermi*, respectively, where we assumed the *Fermi* sensitivity to be $F_{\text{lim}} = 2 \times 10^{-9}$ photons $\text{cm}^{-2} \text{s}^{-1}$ above 100 MeV. This is a standard sensitivity often used in the literature (e.g., Oh 2001; NT06; Venters & Pavlidou 2007), and close to $\sim 5\sigma$ limit for a point source at high Galactic latitude after a 1 year survey. See also the official Science Requirement Document of *Fermi* available at <http://fermi.gsfc.nasa.gov/science/> for the *Fermi* performance. Here, we calculated simply all the blazars without taking into account the probability of identification by follow-up observations in other wavebands. This is why the number of bright blazars is larger than the EGRET observation in Fig. 8; we have taken into account the probability of blazar identification by detecting a radio counterpart in the likelihood analysis of the EGRET blazars. The model of Stecker & Salamon (1996), and the PLE and LDDE models in Narumoto & Totani (2006) predicted ~ 10000 , 5400, and 3000 blazars for the same sensitivity limit, respectively. It is remarkable that the GLF models in this work predict significantly smaller numbers of blazars than previous studies. This is probably because of the SED model newly used here; the IC component has its broad SED peak at around 100 MeV, and the flux at lower and higher energy band is relatively lower than the case of power-law SED, because of the curvature of the spectrum.

The right panel of Figure 8 shows the differential flux distribution of gamma-ray blazars multiplied by flux, showing the contribution to the EGRB per unit logarithmic flux interval. From this plot one can estimate how much fraction of EGRB will be resolved by the *Fermi* mission. The peak of the contribution to EGRB occurs at a flux much brighter than the *Fermi* limit, meaning that EGRB from blazars should practically be resolved into discrete sources. We find that the fraction of EGRB flux that should be resolved is 99, 98, 100, and 100% against the total blazar EGRB flux in the four GLF models of $U03(q)$, $U03(q, \gamma_1)$, $H05(q)$, and $H05(q, \gamma_1)$, respectively. However, as seen in Fig. 7, there is a considerable contribution from non-blazar AGNs to the EGRB flux at 100 MeV, and our next interest is how much fraction of EGRB from non-blazars will be resolved by *Fermi*.

The left panel of Figure 9 shows the cumulative flux distribution of blazars in the $U03(q, \gamma_1)$ model, non-blazar AGNs, and the total of the two. The expected number of non-blazar AGNs detectable by EGRET is much smaller than unity in all sky, and it is consistent with the fact that almost all extragalactic gamma-ray sources detected by EGRET are blazars. However, about 1–30 non-blazar AGNs would be detected by *Fermi*, by their soft nonthermal emission from nonthermal electrons in coronae of accretion disks, giving an interesting test for our model. In fact, we can estimate the > 100 MeV gamma-ray flux from the observed hard X-ray flux of NGC 4151 (the brightest Seyfert galaxy in all sky, Sazonov et al. 2007) using the ITU08 model, and it becomes $\sim 3.3 \times 10^{-8}$ and 4.1×10^{-9} photons $\text{cm}^{-2} \text{s}^{-1}$ for $\Gamma = 3.5$ and 3.8, respectively. Therefore NGC 4151 is marginally detectable when $\Gamma = 3.8$, and easily detectable with $\Gamma = 3.5$, which are nicely consistent with the predicted source counts of non-blazar AGNs detectable by *Fermi*.

On the other hand, the right panel of Figure 9 indicate that EGRB from non-blazar AGNs is hardly resolved into discrete sources by *Fermi*. The predicted fraction of non-blazar EGRB flux resolved by *Fermi* is 0.03 and 0.004 % for the models with $\Gamma = 3.5$ and 3.8, respectively, against the total non-blazar EGRB flux. These results are in sharp contrast to those for blazars, although the contributions to the total EGRB by the two populations are comparable at around 100 MeV. This is because of a large difference between typical absolute luminosities of blazars and non-blazar AGNs. The typical luminosity at 100 MeV of blazars and non-blazars is $\nu L_\nu = 10^{48.0}$ and $10^{42.5}$ erg/s, which are corresponding to L_x^* in the AGN XLF. If the evolution is similar for the two population, the characteristic redshift or distance to the sources having main contribution to EGRB should be similar. Therefore, a source population with smaller characteristic luminosity is more difficult to resolve into discrete sources when the flux sensitivity is fixed.

The above results mean that a considerable part of EGRB at around 100 MeV will remain unresolved even with the *Fermi* sensitivity, because there is a considerable contribution from non-blazar AGNs to EGRB at ~ 100 MeV. However, the contribution from non-blazars should rapidly decrease with increasing photon energy, and almost all of the total EGRB flux at $\gtrsim 1$ GeV should be resolved into discrete blazars by *Fermi*, if there is no significant source contributing to EGRB other than blazars. It should be noted that these predictions can be tested by *Fermi* relatively easily, without follow-up or cross check at other wavebands, once measurements of source counts and EGRB flux have been done by the *Fermi* data. Therefore this gives a simple and clear test for the theoretical model presented here.

6.2. Redshift and Luminosity Distribution

Figure 10 shows the redshift and luminosity distributions of blazars that will be detected by *Fermi*, where we have again set the *Fermi* sensitivity limit as $F_{\text{lim}} = 2 \times 10^{-9}$ photons $\text{cm}^{-2} \text{s}^{-1}$ above 100 MeV. Since we normalized the total number of detectable blazars, only the shapes of distribution should be compared.

It is somewhat surprising that the predicted distributions for *Fermi* are not much different from the observed distributions for EGRET blazars. The redshift distribution of EGRET blazars has already extended to cosmologically significant range of $z \gtrsim 1$, and the normalized distribution at the high- z end does not significantly change by the *Fermi* sensitivity. However, the absolute number of high- z blazars will be increased, because the total number of blazars will drastically be increased by *Fermi* from that of EGRET blazars, although the normalized redshift distributions are similar.

There are some differences in the predictions by the four different GLF models. Since the *Fermi* will dramatically increase the statistics by a large number of detected blazars, a detailed comparison between the GLF models and the *Fermi* data will provide us a quantitative view of the evolutionary nature of blazar GLF, once the redshifts of *Fermi* blazars are measured. The comparison between the blazar GLF and other AGN LFs in different wavebands (e.g., X-ray, optical, and radio) will give us important information about the jet activity evolution of AGNs, in comparison with the evolution of mass accretion history onto SMBH that can be probed by disk luminosity function.

7. CONCLUSIONS

In this paper, we constructed a new model of the blazar gamma-ray luminosity function (GLF), taking into account the blazar SED sequence and the LDDE luminosity function inferred from X-ray observations of AGNs. An implicit assumption here is that the jet activity of AGNs is associated with the accretion activity, and hence the blazar luminosity function has a similar evolution to that of X-ray AGNs. The GLF model parameters are constrained by fitting to the observed flux and redshift distribution of the EGRET blazars. By this model, for the first time, we can predict the spectrum of the extragalactic gamma-ray background (EGRB) in a non-trivial way, rather than assuming a simple functional form such as power-law spectra.

The absorption of gamma-rays in IGM by interaction with the cosmic infrared background (CIB), and the reprocessed cascade emission from electrons/positrons produced in IGM are also taken into account in the EGRB calculation. We found that, provided that the blazar SED sequence is valid, the amount of EGRB energy flux absorbed by CIB interaction (at photon energy $\gtrsim 10$ GeV) is not large and the EGRB spectrum at lower photon energy bands is not significantly affected by the secondary cascade emission.

The contribution from non-blazar AGNs to EGRB is also considered, by using the nonthermal coronal electron model of Inoue et al. (2008). This model is a natural extension of the standard X-ray spectral model of AGN emission from the disk and corona region, and predicts the nonthermal emission extending from MeV to higher energy band with a steep power-law. This model gives a natural explanation for the observed cosmic MeV background, and we examined whether X-ray to GeV gamma-ray background radiation can be accounted for by the two population model including blazars and non-blazar AGNs.

The predicted EGRB flux at 100 MeV by the sum of blazars and non-blazar AGNs can account for more than 80% of the observed EGRB flux of Strong et al. (2004a), and the predicted spectrum is also in good agreement with the observed data from X-ray to ~ 1 GeV, indicating that the EGRB below 1 GeV can mostly be explained by our two population model. The predicted EGRB flux at 100 MeV is larger than those in previous studies, which found that only 25–50% of the observed EGRB flux can be explained by blazars. The two components have a comparable contribution to EGRB at ~ 100 MeV, and the blazar component is dominant at the higher energy range while the non-blazar component at the lower. Therefore, the higher EGRB flux at 100 MeV than previous studies is not by change in the EGRB flux from blazars, but by including non-blazar AGNs.

The EGRB spectrum of Strong et al. (2004a) shows a hump beyond 3 GeV, which cannot be explained by our model. The EGRB flux determined originally by the EGRET team (Sreekumar et al. 1998) is higher than our model, and the observed spectrum is harder. However, measurements of EGRB suffer from the uncertainties in the theoretical modeling of the foreground diffuse Galactic emission, and perhaps from systematic errors in the calibration of the EGRET detector above 1 GeV (Stecker et al. 2008). We must await the *Fermi* data to examine these issues and whether an additional, completely different source is necessary to explain all of EGRB. We conclude that most (at least more than 50%), and probably all, of the observed high-energy background radiation from X-ray to 1 GeV spanning 6 orders of magnitude in photon energy can be accounted for by AGNs including blazars.

We predicted the flux distribution of blazars by our model,

and we found that 600–1200 blazars in all sky should be detected by *Fermi*, assuming a sensitivity limit of $F_{\text{lim}} = 2 \times 10^{-9}$ photons $\text{cm}^{-2} \text{s}^{-1}$ above 100 MeV. This number is significantly lower than the predictions of the previous studies. The expected number of the non-blazar AGNs at 100 MeV band is much smaller than unity in all sky at the EGRET sensitivity, but about 1–30 of such population are expected be detected by *Fermi*. *Fermi* should resolve almost all of the EGRB flux from blazars into discrete blazars, with percentages of $\gtrsim 99\%$ depending on the GLF models. On the other hand, less than 0.1% of the EGRB flux from non-blazar AGNs can be resolved into discrete sources. Therefore, we have a clear prediction: *Fermi* will resolve almost all of the EGRB flux into discrete sources at photon energies $\gtrsim 1$ GeV where blazars are dominant, while a significant fraction of the EGRB flux will remain unresolved in the low energy band of $\lesssim 100$ MeV where non-blazar AGNs have a significant contribution. This prediction can be tested only with the source counts and the

EGRB estimates by *Fermi* data.

We also predicted the redshift and absolute luminosity distribution for the *Fermi* blazars. Future *Fermi* data set with measured redshifts will enable us to get a quantitative measurement of the blazar GLF and its evolution with a much larger statistics than EGRET. A direct comparison between blazar GLF and X-ray AGN LF could be done, making it possible to discuss the relation between the cosmic histories of jet activity and accretion activity of AGNs. Our model will be able to serve as a guide in such studies.

We thank Takuro Narumoto and Tuneyoshi Kamae for their help and useful discussions. This work was supported by the Grant-in-Aid for the Global COE Program "The Next Generation of Physics, Spun from Universality and Emergence" from the Ministry of Education, Culture, Sports, Science and Technology (MEXT) of Japan.

REFERENCES

- Aharonian, F. A., Coppi, P. S., & Voelk, H. J. 1994, *ApJ*, 423, L5
 Ajello, M., et al. 2008, ArXiv e-prints, 808, arXiv:0808.3377
 Chiang, J., Fichtel, C. E., von Montigny, C., Nolan, P. L., & Petrosian, V. 1995, *ApJ*, 452, 156
 Chiang, J. & Mukherjee, R. 1998, *ApJ*, 496, 752
 de Boer, W., Sander, C., Zhukov, V., Gladyshev, A. V., & Kazakov, D. I. 2005, *A&A*, 444, 51
 Dermer, C. D. 2007, *ApJ*, 659, 958
 Dermer, C. D. & Schlickeiser, R. 1993, *ApJ*, 416, 458
 Donato, D., Ghisellini, G., Tagliaferri, G., & Fossati, G. 2001, *A&A*, 375, 739 (D01)
 Fan, Y. Z., Dai, Z. G., & Wei, D. M. 2004, *A&A*, 415, 483
 Fichtel, C. E., Simpson, G. A., & Thompson, D. J. 1978, *ApJ*, 222, 833
 Fossati, G., Celotti, A., Ghisellini, G., & Maraschi, L. 1997, *MNRAS*, 289, 136
 Fossati, G., Maraschi, L., Celotti, A., Comastri, A., & Ghisellini, G. 1998, *MNRAS*, 299, 433
 Gallo, E., Fender, R., Kaiser, C., Russell, D., Morganti, R., Oosterloo, T., & Heinz, S. 2005, *Nature*, 436, 819
 Gallo, E., Fender, R. P., & Pooley, G. G. 2003, *MNRAS*, 344, 60
 Ghisellini, G., & Tavecchio, F. 2008, *MNRAS*, 387, 1669
 Gilli, R., Comastri, A., & Hasinger, G. 2007, *A&A*, 463, 79
 Giommi, P., Colafrancesco, S., Cavazzuti, E., Perri, M., & Pittori, C. 2006, *A&A*, 445, 843
 Gruber, D. E., Matteson, J. L., Peterson, L. E., & Jung, G. V. 1999, *ApJ*, 520, 124
 Hasinger, G., Miyaji, T., & Schmidt, M. 2005, *A&A*, 441, 417 (H05)
 Inoue, Y., Totani, T., & Ueda, Y. 2008, *ApJ*, 672, L5 (ITU08)
 Kamae, T., Abe, T., & Koi, T. 2005, *ApJ*, 620, 244
 Kamae, T., Karlsson, N., Mizuno, T., Abe, T., & Koi, T. 2006, *ApJ*, 647, 692
 Kappadath, S. C., et al. 1996, *A&AS*, 120, C619+
 Kato, S., Fukue, J., & Mineshige, S., eds. 1998, *Black-hole accretion disks*
 Keshet, U., Waxman, E., & Loeb, A. 2004, *Journal of Cosmology and Astro-Particle Physics*, 4, 6
 Kneiske, T. M., Bretz, T., Mannheim, K., & Hartmann, D. H. 2004, *A&A*, 413, 807
 Kneiske, T. M. & Mannheim, K. 2008, *A&A*, 479, 41
- Laor, A. & Behar, E. 2008, ArXiv e-prints, 808
 MAGIC Collaboration, Albert, et al. 2008, *Science*, 320, 1752
 Maraschi, L., Foschini, L., Ghisellini, G., Tavecchio, F., & Sambruna, R. M. 2008, arXiv:0810.0145
 Marconi, A., Risaliti, G., Gilli, R., Hunt, L. K., Maiolino, R., & Salvati, M. 2004, *MNRAS*, 351, 169
 Mücke, A. & Pohl, M. 2000, *MNRAS*, 312, 177
 Narayan, R. & Quataert, E. 2005, *Science*, 307, 77
 Narumoto, T. & Totani, T. 2006, *ApJ*, 643, 81
 Oda, T., Totani, T., & Nagashima, M. 2005, *ApJ*, 633, L65
 Oh, S. P. 2001, *ApJ*, 553, 25
 Padovani, P., Ghisellini, G., Fabian, A. C., & Celotti, A. 1993, *MNRAS*, 260, L21
 Padovani, P., Giommi, P., Landt, H., & Perlmutter, E. S. 2007, *ApJ*, 662, 182
 Pavlidou, V. & Vinters, T. M. 2008, *ApJ*, 673, 114
 Pohl, M. & Esposito, J. A. 1998, *ApJ*, 507, 327
 Protheroe, R. J. 1986, *MNRAS*, 221, 769
 Salamon, M. H. & Stecker, F. W. 1994, *ApJ*, 430, L21
 —. 1998, *ApJ*, 493, 547
 Sazonov, S., Revnivtsev, M., Krivonos, R., Churazov, E., & Sunyaev, R. 2007, *A&A*, 462, 57
 Sreekumar, P., et al. 1998, *ApJ*, 494, 523
 Stecker, F. W., Hunter, S. D., & Kniffen, D. A. 2008, *Astroparticle Physics*, 29, 25
 Stecker, F. W., Malkan, M. A., & Scully, S. T. 2006, *ApJ*, 648, 774
 Stecker, F. W. & Salamon, M. H. 1996, *ApJ*, 464, 600
 Stecker, F. W., Salamon, M. H., & Malkan, M. A. 1993, *ApJ*, 410, L71
 Strong, A. W., Moskalenko, I. V., & Reimer, O. 2004a, *ApJ*, 613, 956
 —. 2004b, *ApJ*, 613, 962
 Thompson, D. J. & Fichtel, C. E. 1982, *A&A*, 109, 352
 Totani, T. & Takeuchi, T. T. 2002, *ApJ*, 570, 470
 Ueda, Y., Akiyama, M., Ohta, K., & Miyaji, T. 2003, *ApJ*, 598, 886 (U03)
 Vinters, T. M., & Pavlidou, V. 2007, *ApJ*, 666, 128
 Watanabe, K., Hartmann, D. H., Leising, M. D., & The, L.-S. 1999, *ApJ*, 516, 285

APPENDIX

THE BLAZAR SED SEQUENCE FORMULATIONS

We define $\psi(x) \equiv \log_{10}[\nu L_{\nu}/(\text{erg s}^{-1})]$ with $x \equiv \log_{10}(\nu/\text{Hz})$ (ν in rest-frame). The empirical SED sequence model of blazars is the sum of the synchrotron $[\psi_s(x)]$ and IC $[\psi_c(x)]$ emissions, i.e.,

$$\psi(x) = \log_{10}[10^{\psi_s(x)} + 10^{\psi_c(x)}]. \quad (\text{A1})$$

Each of the two components is described by a combination of a linear and a parabolic functions at low and high photon frequencies, and we define $x_{\text{tr},s}$ and $x_{\text{tr},c}$ as the linear-parabolic transition frequencies for the synchrotron and IC components, respectively. We take $\psi_R \equiv \log_{10}[L_R/(\text{erg s}^{-1})]$ as a reference of a blazar luminosity, where L_R is νL_{ν} luminosity in the radio band ($\nu_R = 5$ GHz or $x_R = 9.698$). The linear part of the synchrotron component is described as follows:

$$\psi_s(x) = \psi_{s1}(x) \equiv (1 - \alpha_s)(x - x_R) + \psi_R \quad (x < x_{\text{tr},s}), \quad (\text{A2})$$

where $\alpha_s = 0.2$ is the energy flux index (i.e., $L_\nu \propto \nu^{-\alpha_s}$). The parabolic part of the synchrotron component is characterized by the νL_ν peak frequency ν_s (or corresponding x_s), as

$$\psi_s(x) = \psi_{s2}(x) \equiv -[(x - x_s)/\sigma]^2 + \psi_{s,p} \quad (x \geq x_{tr,s}), \quad (A3)$$

where σ is a parameter that controls the width of the parabolic function. The peak luminosity $\psi_{s,p}$ of the synchrotron component is determined if $x_{tr,s}$, x_s , and σ are given, by requiring the continuity between the linear and parabolic parts, i.e., $\psi_{s1}(x_{tr,s}) = \psi_{s2}(x_{tr,s})$. The result is:

$$\psi_{s,p} = (1 - \alpha_s)(x_{tr,s} - x_R) + \left(\frac{x_{tr,s} - x_s}{\sigma} \right)^2 + \psi_R. \quad (A4)$$

The linear part of the IC component (roughly in the hard X-ray band) is defined as:

$$\psi_c(x) = \psi_{c1}(x) \equiv (1 - \alpha_c)(x - x_X) + \psi_X \quad (x < x_{tr,c}), \quad (A5)$$

where the power index is $\alpha_c = 0.6$ (different from the synchrotron component), and ψ_X is the luminosity of IC component at the reference frequency $\nu_X = 2.42 \times 10^{17}$ Hz = 1 keV/ h_p ($x_X = 17.383$). The parabolic part of the IC component is characterized by the νL_ν peak frequency ν_c (or corresponding to x_c) with the same width parameter σ as the synchrotron component, i.e.,

$$\psi_c(x) = \psi_{c2}(x) \equiv -[(x - x_c)/\sigma]^2 + \psi_{c,p} \quad (x \geq x_{tr,c}), \quad (A6)$$

where $\psi_{c,p}$ is the peak luminosity of the IC component. The linear-parabolic transition frequency $x_{tr,c}$ is determined by requiring continuity, $\psi_{c1}(x_{tr,c}) = \psi_{c2}(x_{tr,c})$ and the result is:

$$x_{tr,c} = \frac{-\zeta - \sqrt{\zeta^2 - 4\eta}}{2}, \quad (A7)$$

where

$$\zeta = \sigma^2(1 - \alpha_c) - 2x_c, \quad (A8)$$

$$\eta = x_c^2 + \sigma^2[\psi_X - x_X(1 - \alpha_c) - \psi_{c,p}]. \quad (A9)$$

Then, the SED sequence is determined when $x_{tr,s}$, x_s , σ , ψ_X , x_c , and $\psi_{c,p}$ are given as functions of ψ_R . First we set $x_{tr,s} = \log_{10}(5 \times 10^{10})$ and $10^{x_c - x_s} = \nu_c / \nu_s = 5 \times 10^8$, for all luminosity range of blazars. To get a good fit in all luminosity range, we divide the luminosity into two ranges of $\psi_R \leq 43$ and $\psi_R > 43$. The parameters relevant for the synchrotron component in the $\psi_R \leq 43$ range are determined as follows. The synchrotron peak frequency is determined by

$$x_s = -\xi(\psi_R - 43) + 14.47, \quad (A10)$$

with $\xi = 0.88$. The width parameter σ is determined by the following scaling law:

$$\sigma = 0.0891 x_s + 1.78. \quad (A11)$$

In this case, the connection at $x = x_{tr,s}$ is not smooth (i.e., not differentiable), but the discontinuity of the derivative is not significant. In the range of $\psi_R > 43$, we change the synchrotron peak frequency x_s by adopting $\xi = 0.4$, and the width parameter σ is determined so that the connection at $x_{tr,s}$ is differentiable, i.e.,

$$\sigma = [2(x_s - x_{tr,s}) / (1 - \alpha_s)]^{1/2}. \quad (A12)$$

For the IC component parameters, the IC peak luminosity $\psi_{c,p}$ is assumed to be the same as the synchrotron peak, i.e., $\psi_{c,p} = \psi_{s,p}$, at $\psi_R \leq 43$, while it is determined by the following formula at $\psi_R > 43$:

$$\psi_{c,p} = \beta(\psi_R - 43)^\delta + \epsilon, \quad (A13)$$

where $\beta = 1.77$, $\delta = 0.718$, and $\epsilon = 45.3$. Still, the normalization of the IC linear part, ψ_X , remains to be determined. To get a good fit to the X-ray data, we define the dependence of this parameter on ψ_R as follows:

$$\psi_X = \begin{cases} (\psi_R - 43) + \psi_{X,43} & (\psi_R \leq 43) \\ 1.40(\psi_R - 43) + \psi_{X,43} & (43 < \psi_R \leq 46.68) \\ 1.40(46.68 - 43) + \psi_{X,43} & (46.68 < \psi_R) \end{cases} \quad (A14)$$

with $\psi_{X,43} = 43.17$. The parameter ψ_X is kept constant at $\psi_R > 46.68$, because $\psi_{c1}(x) = \psi_{c2}(x)$ does not have solution and hence $x_{tr,c}$ cannot be obtained, when we extrapolate the ψ_X formula at $\psi_R \leq 46.68$ into $\psi_R > 46.68$. At $\psi_R = 46.68$, $\psi_{c,p}$ becomes 49.81, which is brighter than the maximum L_γ of the EGRET blazars, and is larger than the characteristic L_γ^* corresponding to the break X-ray luminosity L_X^* in the AGN XLF by a factor of ~ 60 . Therefore, the treatment of ψ_X at such large luminosity range is not important when we consider the overall properties of blazars and EGRB. The linear-parabolic connection of the IC component at $x_{tr,c}$ is not as smooth as that of the synchrotron component at $x_{tr,s}$, but this is inevitable to fit the SED in the X-ray region.

It should be noted that the formulations of x_s , σ , $\psi_{c,p}$, and ψ_X are continuous at $\psi_R = 43$ and 46.68. Therefore the SED in this formula always changes continuously with ψ_R in the whole luminosity range, which was the motivation of constructing this new formulation.

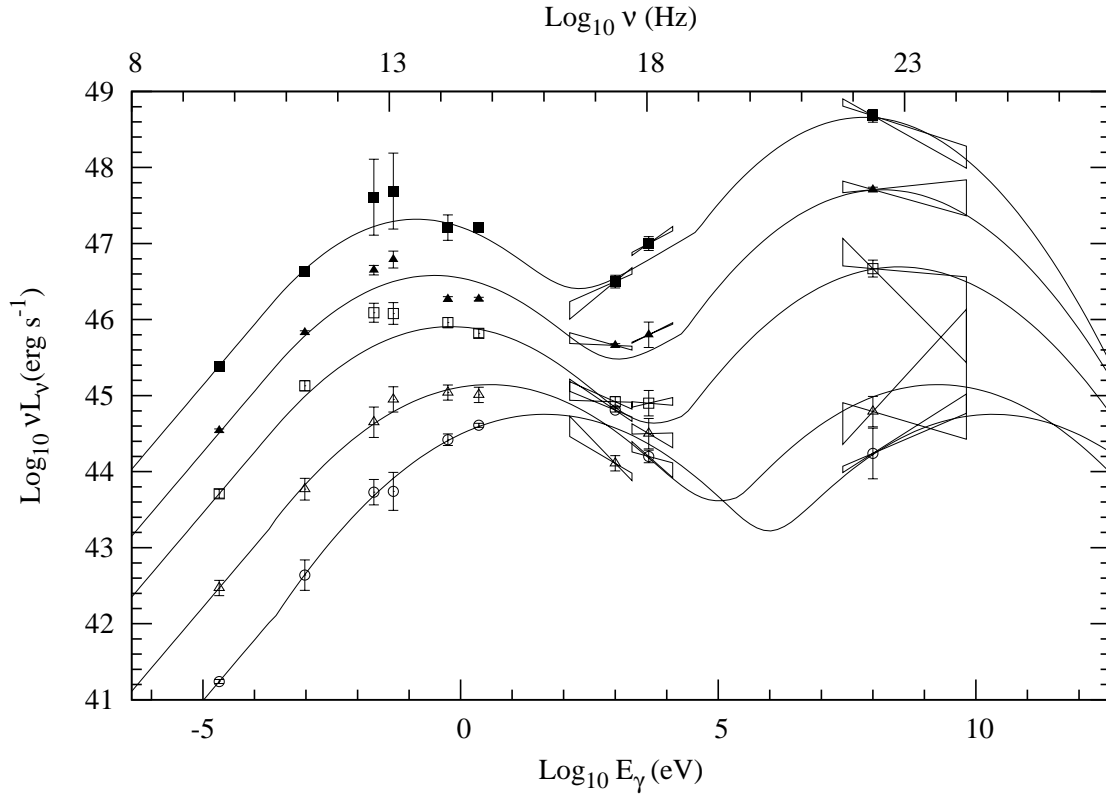


FIG. 1.— The blazar SED sequence. The data points are the average SED of the blazars studied by Fossati et al. (1998) and D01. The solid curves are the empirical SED sequence models constructed and used in this paper. The model curves corresponds to the bolometric luminosities of $\log_{10}(P/\text{erg s}^{-1}) = 49.50, 48.64, 47.67, 46.37, \text{ and } 45.99$ (from top to bottom).

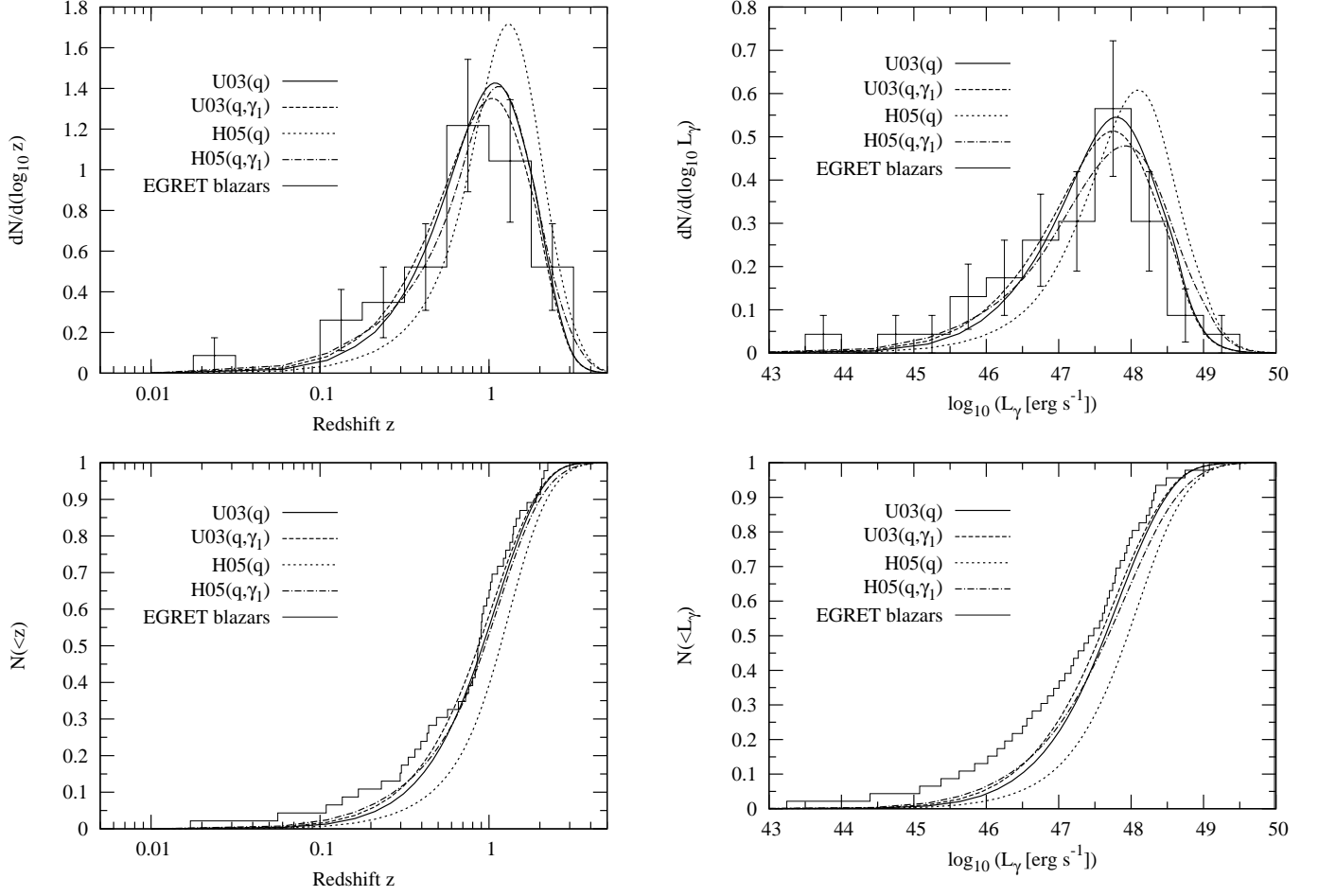


FIG. 2.— Top panels: redshift and gamma-ray luminosity (νL_ν at 100 MeV) distributions of EGRET blazars. The histogram is the binned EGRET data, with one sigma Poisson errors. The four model curves are the best-fits for the GLF models of U03(q), H05(q), U(q, γ_1), and H05(q, γ_1), as indicated in the figure. Bottom panels: the same as the top panels, but for cumulative distributions.

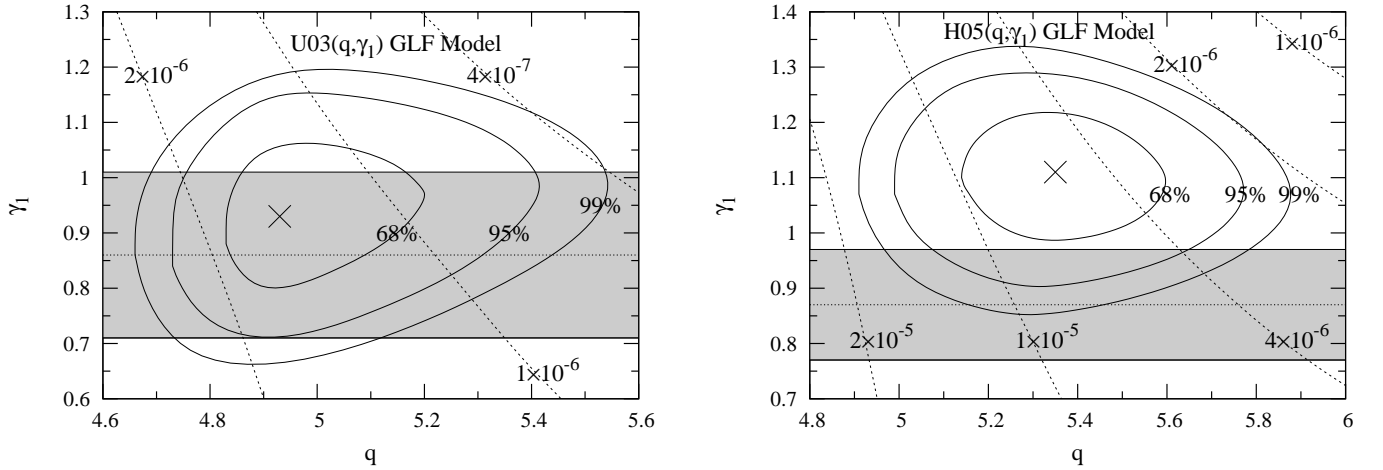


FIG. 3.— *Left:* Solid contours show the 68%, 95%, and 99% CL likelihood contours for the LDDE model parameters [the faint-end slope index, γ_1 , and the ratio of the blazar emission power to X-ray luminosity, q] in the case of the U03 XLF. The best-fit values $(q, \gamma_1) = (4.93, 0.93)$ are shown by the cross. The dotted contours are for the parameter κ , the normalization ratio of blazar GLF to AGN XLF. The κ values for the contours are indicated in the figure. The shaded region indicates the error region of the original γ_1 value determined for AGN XLF by X-ray surveys. *Right:* The same as the left panel, but for the H05 XLF. The best-fit values $(q, \gamma_1) = (5.35, 1.11)$ are shown by the cross.

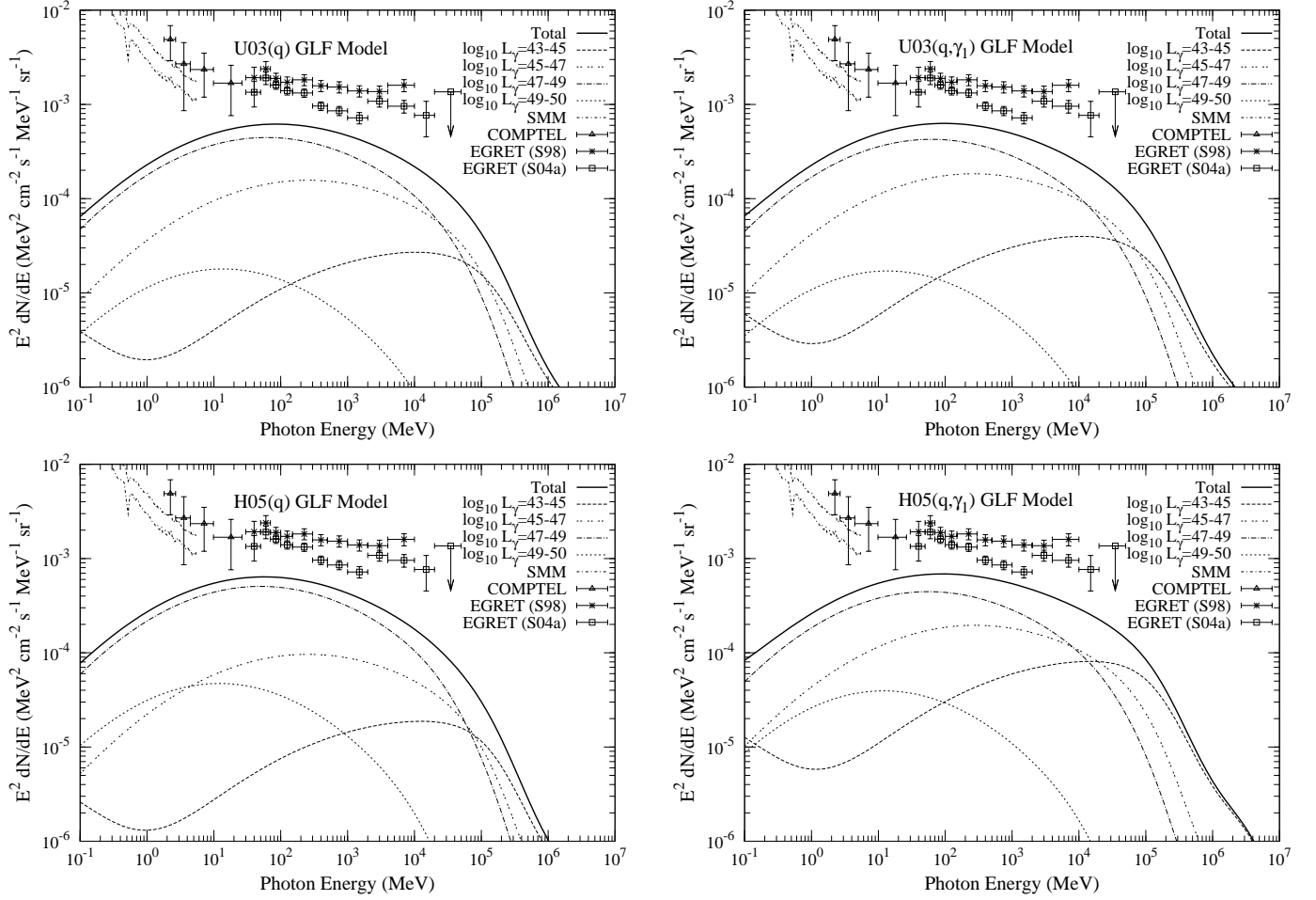


FIG. 4.— The blazar EGRB spectrum (energy flux per unit logarithmic photon energy and per steradian). The four panels are for the four different GLF models of U03(q), U03(q, γ_1), H05(q), and H05(q, γ_1). The solid curve is for the total EGRB spectrum from all blazars, and the other curves are for a particular range of blazar luminosity, as indicated in the figure (L_γ in units of erg/s). The effect of absorption by CIB is included, while the reprocessed cascade component is not included. The observed data of SMM (Watanabe et al. 1999), COMPTEL (Kappadath et al. 1996), and EGRET [Sreekumar et al. 1998 (S98); Strong et al. 2004a (S04a)] experiments are also shown with the symbols indicated in the figure.

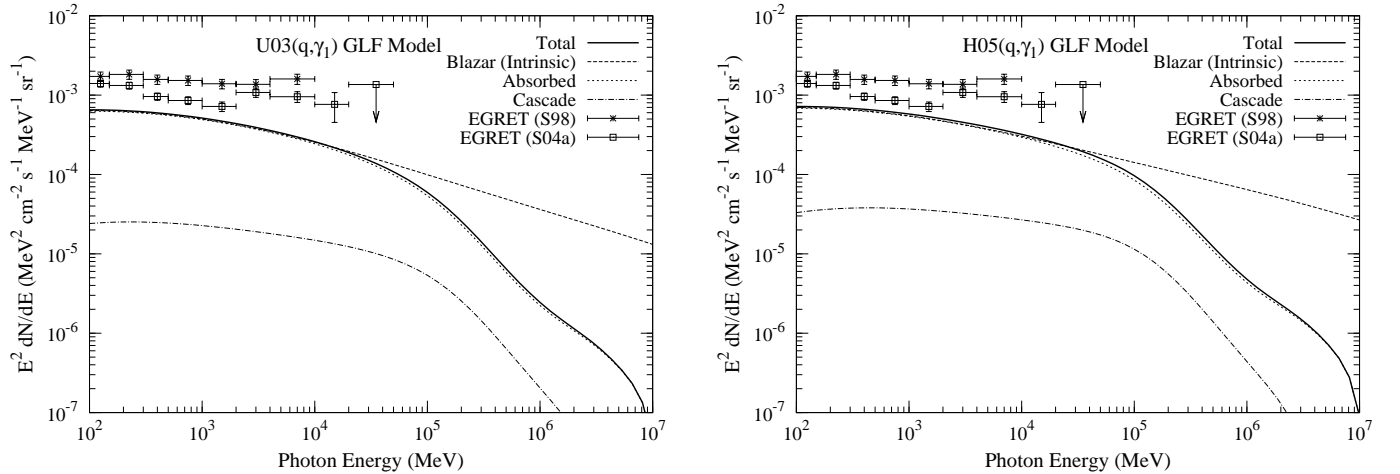


FIG. 5.— The blazar EGRB spectrum. The two panels are for the two different GLF models of U03(q, γ_1) and H05(q, γ_1). The curves are the model predictions for the intrinsic (no absorption by CIB), absorbed, and cascade (reprocessed emission by electrons/positrons produced in IGM) components of the EGRB spectrum. The solid curve is the total flux, i.e., absorbed plus cascade components. The EGRET data are the same as those in Fig. 4.

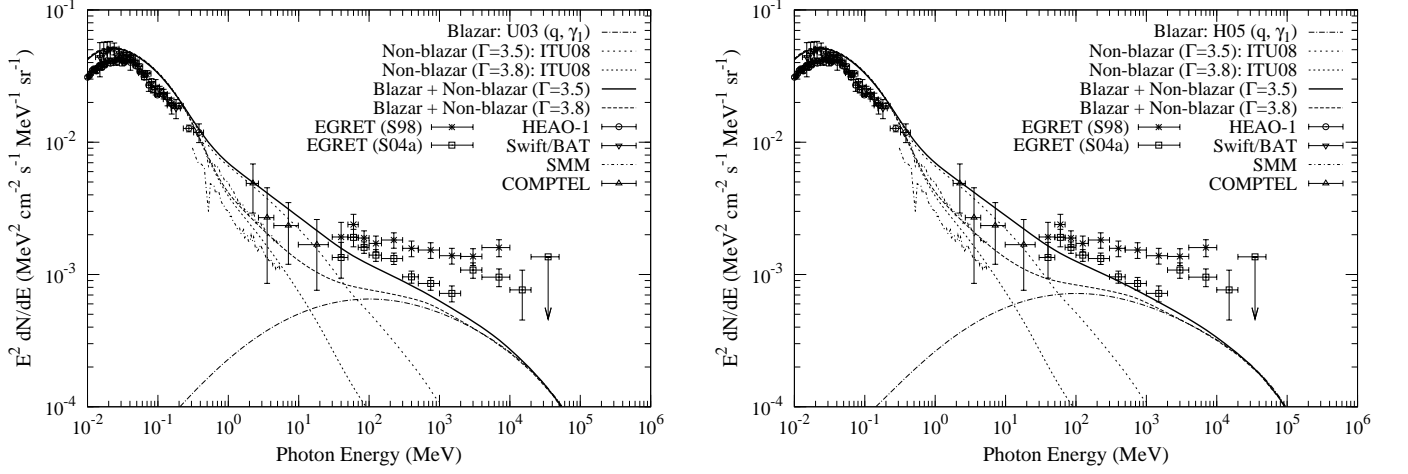


FIG. 6.— The EGRB spectrum from non-blazar AGNs and blazars. The two panels are for the two different blazar GLF models of U03(q, γ_1) (left) and H05(q, γ_1) (right). The model curves of the blazar component (absorbed+cascade), non-blazar AGN component, and the total of the two populations are shown. Note that two models are plotted for the non-blazar component with different values of Γ (see the line-markings indicated in the figure). The observed data of HEAO-1 (Gruber et al. 1999) and *Swift*/BAT (Ajello et al. 2008) are shown. The other data are the same as those in Fig. 4.

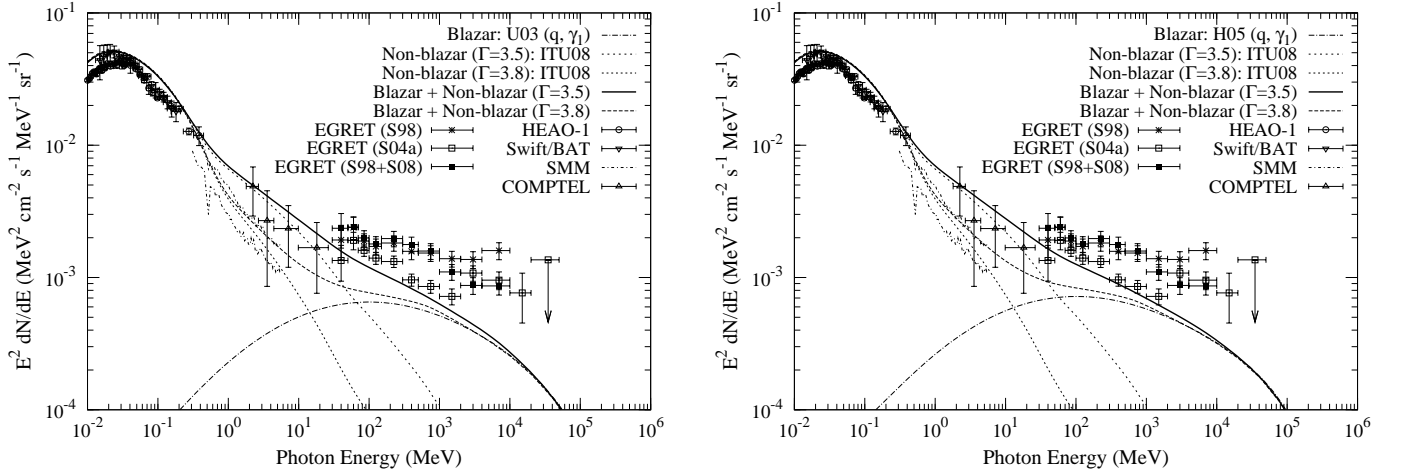


FIG. 7.— The same as Fig. 6, but with a new EGRET data denoted as “S98+S08”, which is the original EGRET determination of Sreekumar et al. (1998) corrected by the correction factors proposed by Stecker et al. (2008, S08). The other data are the same as those in Fig. 4.

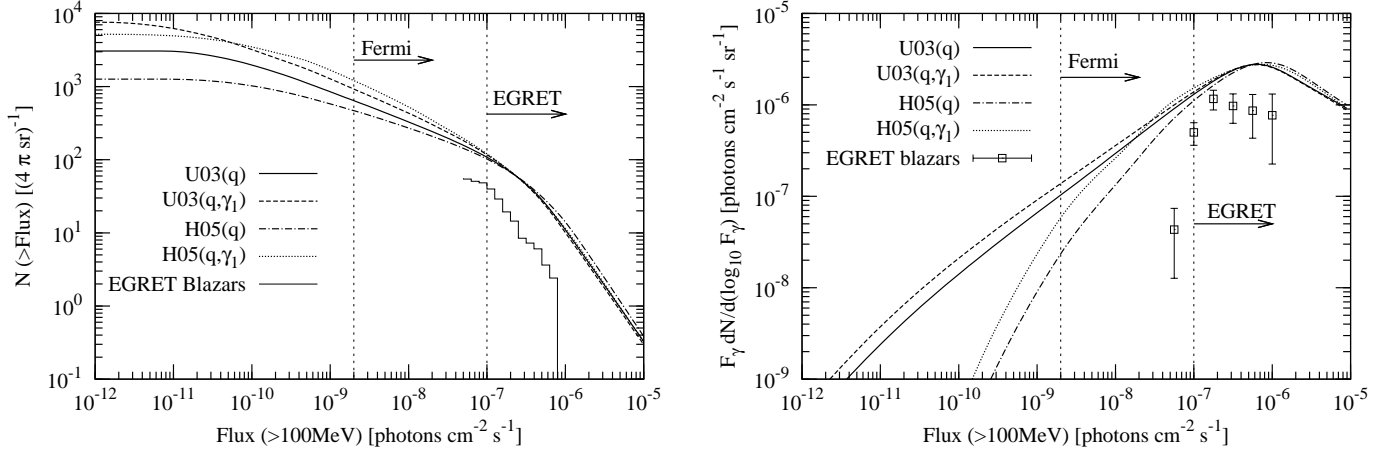


FIG. 8.— Left: the cumulative flux distribution of blazars. The four model curves correspond to the four different GLF models of U03(q), H05(q), U(q, γ_1), and H05(q, γ_1) are shown. The thin solid line shows the observed distribution of EGRET blazars. The detection limits of EGRET and *Fermi* are also shown. Right: the same as the left panel, but showing differential flux distribution multiplied by flux F_γ , to show the contribution to EGRB per logarithmic flux interval. The solid squares are the EGRET data with Poisson errors.

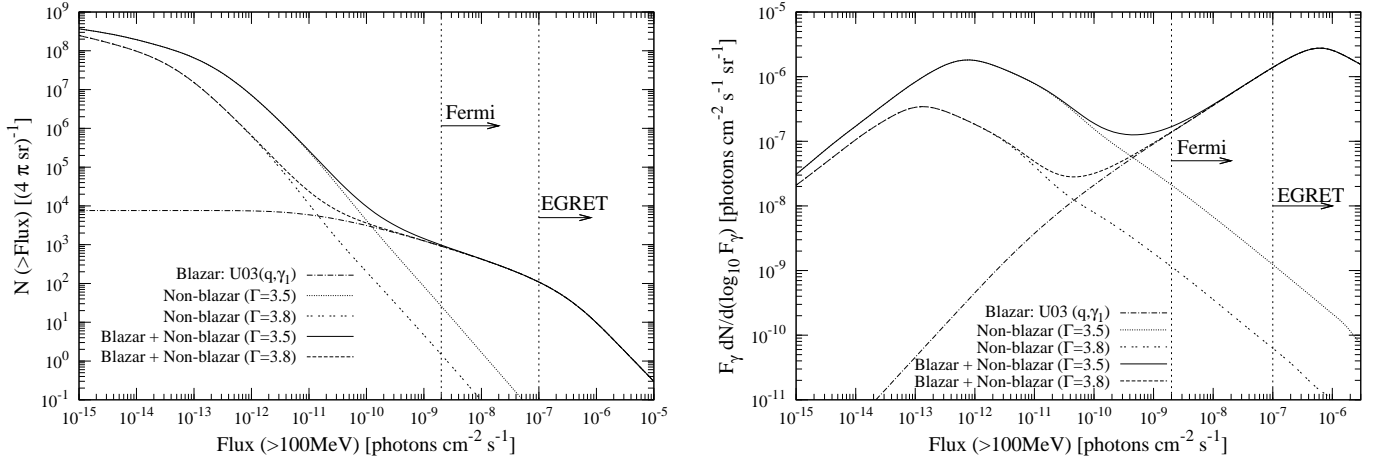


FIG. 9.— The same as Fig. 8, but showing non-blazar AGNs as well, in addition to blazars. The two models of non-blazar AGNs with different values of Γ are shown. The total of blazar plus non-blazar counts is also shown.

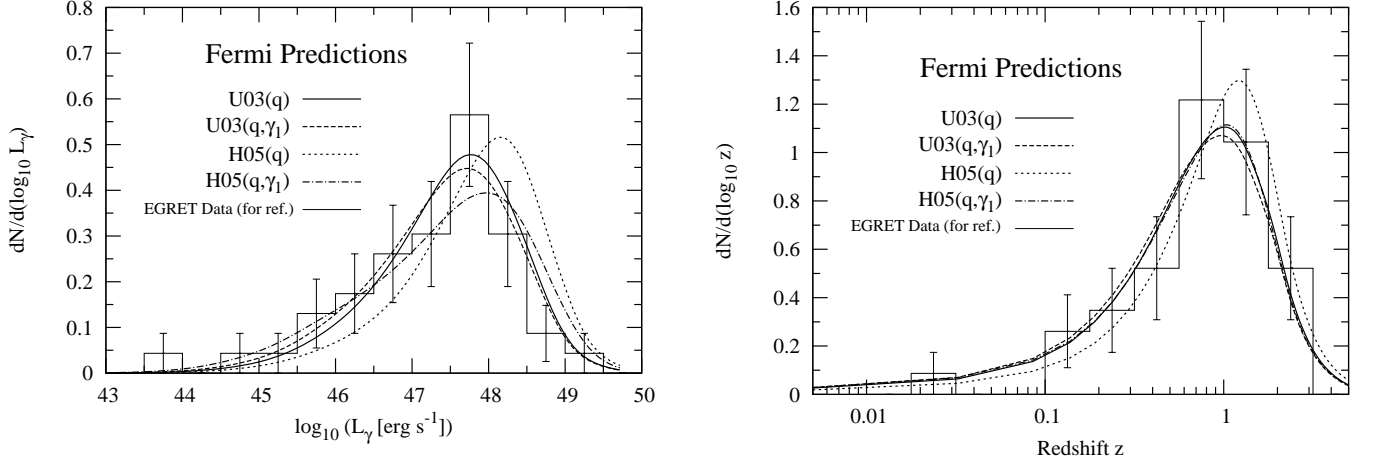


FIG. 10.— The predictions for the redshift and gamma-ray luminosity (νL_ν at rest frame 100 MeV) distributions of blazars for *Fermi*. The four model curves are for the four different GLF models of U03(q), H05(q), U(q, γ_1), and H05(q, γ_1). The *Fermi* sensitivity limit is set as $F_{\text{lim}} = 2 \times 10^{-9}$ photons $\text{cm}^{-2} \text{s}^{-1}$ for photon flux above 100 MeV. The observed distributions of EGRET blazars are shown, for comparison against the expected distributions of *Fermi* blazars.